Article:
Binh, Nguyen Thanh, Ruta, Sergiu, Hovorka, Ondrej et al. (2022) Influence of finite-size effects on the Curie temperature of L10-FePt. Physical Review B. 054421. ISSN: 2469-9969

https://doi.org/10.1103/PhysRevB.106.054421

Influence of finite-size effects on the Curie temperature of $L1_0$-FePt

Nguyen Thanh Binh [1,*] Sergiu Ruta [1] Ondrej Hovorka [2] Richard F. L. Evans [1] and Roy W. Chantrell [1]

[1]*Department of Physics, The University of York, Heslington, York YO10 5DD, England, United Kingdom*

[2]*Faculty of Engineering and Physical Sciences, The University of Southampton, Southampton SO17 1BJ, England, United Kingdom*

(Received 13 March 2022; revised 11 July 2022; accepted 15 July 2022; published 17 August 2022)

We employ an atomistic model using a nearest-neighbor Heisenberg Hamiltonian exchange to study computationally the dependence of the Curie temperature of $L1_0$-FePt on finite-size and surface effects in heat-assisted magnetic recording (HAMR) media. We demonstrate the existence of a size threshold at 3.5 nm below which the impact of finite-size effects starts to permeate into the center of the grains and contributes to the reduction of the Curie temperature. We find a correlation between the Curie temperature and the percentage of atomistic bonds lost on the surface as a function of grain size, which can be extended to apply to not only $L1_0$-FePt but also generic magnetic systems of any crystal structure. In a recording medium, the inevitable grain size dispersion leads to an irreducible contribution to the dispersion of the Curie temperature. Therefore, our paper gives insight into finite-size effects, which have been predicted to be a serious limitation of HAMR.

DOI: 10.1103/PhysRevB.106.054421

I. INTRODUCTION

Magnetic recording functions on the balance between three main factors which form the well-known magnetic trilemma: The task of optimizing the signal-to-noise (SNR) ratio, thermal stability, and writability [1]. To improve areal density while maintaining sufficient SNR, the grain volume in the recording medium is reduced, leading potentially to a loss of thermal stability. Hence, the requirement is to find a recording layer material with high uniaxial anisotropy energy density K to ensure that the thermal stability factor $KV/kT \geqslant 60$ with V being the grain volume. However, using a high-anisotropy material for the recording medium produces yet another issue: That a high magnetic field from the writing transducer would be required to switch the grain magnetization. In principle, a fourth factor has to be taken into account: A probability of back-switching of spins during the assisted-writing process due to thermally induced transitions. Currently this acts as a source of DC noise, however in terms of ultrahigh storage densities involving heated dot recording this gives a potential limit of magnetic recording density [2].

Recently, heat-assisted magnetic recording (HAMR) has emerged as a solution to circumvent the problem presented by the magnetic trilemma [3,4]. The HAMR writing head first applies an intense, highly localized heat spot for a very short time to a recording medium to heat it up to or beyond its Curie temperature (T_C), then writes the data inductively after which cooling to ambient temperature restores the thermal stability. Among many possible candidates for a HAMR recording layer material, iron platinum in the $L1_0$ phase ($L1_0$-FePt) has been regarded as an excellent choice [5]. $L1_0$-FePt has been widely studied for application in HAMR in which $L1_0$-FePt can function either as a single layer or as part of a composite multilayer recording medium [6–11]. FePt undergoes a transition at around 300°C from the bulk alloy A1 phase with a disordered, randomly distributed face-centered-cubic (fcc) crystal structure to a chemically ordered face-centered-tetragonal (fct) crystal structure in the $L1_0$ phase [12]. In the $L1_0$ phase, FePt is composed of alternating layers of 3d-element Fe and 5d-element Pt atoms along the (001) direction as sketched in Fig. 1. In the $L1_0$ phase the Fe spins polarize the Pt spins the large spin-orbit coupling of which results in the very high magnetic uniaxial anisotropy necessary for the thermal stability of written information [5,13].

Simulations by Li and Zhu [14,15] have shown that the dispersion of T_C is a serious limitation for the ultimate storage density achievable for HAMR. Consequently, a crucial aspect for successful HAMR media is controlling the Curie temperature dispersion of the recording medium. However, the exact Curie temperature of $L1_0$-FePt has yet to be established; rather, it has been reported to fall between 650 and 780 K under various treatments and measurements [16]. Also, the Curie temperature of $L1_0$-FePt has been shown to drop rapidly with decreasing grain size [17–19]. Consequently, in a recording medium using $L1_0$-FePt the grain size distribution which always exists would inevitably lead to an irreducible dispersion of Curie temperature σ_{T_C} which potentially limits the recording density. Therefore, it poses an important question to determine the precise dependence of the Curie temperature distribution in $L1_0$-FePt grains on finite-size effects as well as the governing mechanisms behind it.

In this paper, we present a computational investigation of the impact of finite-size effects in $L1_0$-FePt grains using a nearest-neighbor Heisenberg Hamiltonian atomistic spin model in which short-range exchange interactions are assumed to dominate. Although the exchange interactions in FePt are long-ranged, Waters *et al.* [16] have shown that the critical exponent of FePt conforms to the three-dimensional

*Corresponding author: btn500@york.ac.uk

Heisenberg universality class. Our starting point is the consideration of thermal fluctuations, which can modify T_C and even shift the ground state solutions to induce changes in magnetic phases. To see this, one needs to look at how the free energy changes as a function of system size. Generally, the free energy will have a functional part reflecting the surface effects due to reduced coordination number, but there will be another term that will correspond to renormalization of state energies resulting from fluctuations [20]. Which one is more important will depend on the system and the size. We hypothesize a correlation between the Curie temperature distribution of $L1_0$-FePt and the percentage of atomistic bond loss on the surface of the grains as a function of grain size, which allows us to quantify the distinct surface and fluctuation contributions to the finite-size effects. We find that our hypothesized correlation could be extended to encompass the role of crystal structures, which suggests it is not restricted to $L1_0$-FePt specifically but universally applicable for any generic magnetic system.

II. THEORIES

Here we describe the two main theories used in our calculation: The atomistic spin model and the mean-field model.

A. Atomistic spin model

Numerical simulations are first carried out using an atomistic spin model. The energy of a magnetic system is generally described in terms of the Hamiltonian $\mathcal{H}$ as the sum of all energy contributions. The three most important contributors include the exchange interaction between pairs of local spins $\mathcal{H}_{\text{exchange}}$, the magnetic uniaxial anisotropy $\mathcal{H}_{\text{anisotropy}}$, and the externally applied magnetic field $\mathcal{H}_{\text{field}}$. The explicit forms of these terms in the Hamiltonian are given as follows:

$$\mathcal{H} = -\frac{1}{2}\sum_{i,j} J_{ij}\,(\hat{\mathbf{s}}_i \cdot \hat{\mathbf{s}}_j) - k_u \sum_i (\hat{\mathbf{s}}_i \cdot \hat{\mathbf{e}})^2 - \sum_i \mu_i (\hat{\mathbf{s}}_i \cdot \mathbf{B}), \tag{1}$$

where J_{ij} is the exchange energy strength between $\hat{\mathbf{s}}_i$ and $\hat{\mathbf{s}}_j$ – the unit vector of local spin at site i and j respectively; k_u is the uniaxial anisotropy constant having an easy direction along $\hat{\mathbf{e}}$, μ_i is the atomic spin moment, and $\mathbf{B}$ is the externally applied magnetic field.

The Hamiltonian of $L1_0$-FePt in principle includes energy contributions from both Fe and Pt components. However, Mryasov *et al.* [13], using Density Functional Theory in the constrained local-spin-density approximation, theoretically demonstrated that the Hamiltonian of $L1_0$-FePt could be rewritten in terms of the Fe degree of freedom only. Using this approach, the original fct-structured $L1_0$-FePt in Fig. 1 can be represented as a simple cubic structured Fe-only system with modified lattice properties – a new configuration henceforth referred to as the modified sc-FePt. An implication immediately follows that it would then be possible to extend the scope of our paper to incorporate the role of different crystal structures beyond the original fct $L1_0$-FePt.

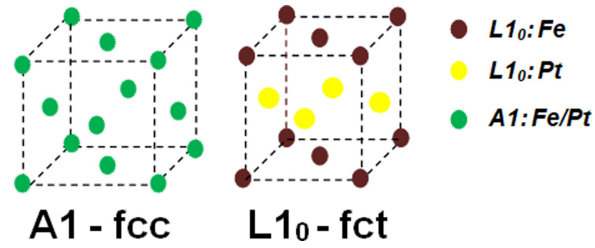

FIG. 1. Crystal structures of FePt: Disordered A1-fcc bulk alloy $Fe_{0.5}Pt_{0.5}$ at room temperature (left) and ordered $L1_0$-fct at HAMR temperature (right).

B. Lattice site resolved mean-field model

Penny *et al.* [21] have shown that a mean-field approach is valuable for the investigation of finite-size effects, including lattice types and particle shapes. To support the interpretation of our atomistic model calculation, we use a lattice site resolved mean-field model outlined as follows [22]. Consider the standard Heisenberg spin Hamiltonian including an exchange term and an applied field $\mathbf{B}$ term. Note that in mean-field treatment the anisotropy term can normally be safely neglected because it has very weak effect on the Curie temperature compared to the exchange. For convenience, we use the same spin notation as [22]:

$$\mathcal{H} = -\frac{1}{2}J\sum_{\langle ij\rangle} \hat{\mathbf{s}}_i \cdot \hat{\mathbf{s}}_j - \mu \sum_i \hat{\mathbf{s}}_i \cdot \mathbf{B}, \tag{2}$$

where the individual terms represent the ferromagnetic exchange interaction energy and the Zeeman energy. The symbol $\langle\cdot\rangle$ in the first sum implies that only the nearest-neighbor spin pairs are summed over. The spin variables are unit vectors $\hat{\mathbf{s}}_i = \boldsymbol{\mu}_i/\mu$, $i = 1, \ldots, N$, where $\boldsymbol{\mu}_i$ is the magnetic moment associated with the spin i and $\mu = |\boldsymbol{\mu}_i|$ is its magnitude.

A conventional way to derive the mean-field approximation is to express the spin variables in Eq. (2) as $\mathbf{s}_i = \tilde{\mathbf{m}}_i + \delta\mathbf{s}_i$, where $\tilde{\mathbf{m}}_i$ and $\delta\mathbf{s}_i$ are, respectively, the thermally averaged and fluctuating parts of the spin variable $\mathbf{s}_i$. Neglect the fluctuations $\delta\mathbf{s}_i$ beyond the first order and rewrite Eq. (2) as

$$\mathcal{H}_{\text{MF}} = \frac{1}{2}J\sum_{\langle ij\rangle} \tilde{\mathbf{m}}_i \cdot \tilde{\mathbf{m}}_j - \sum_i \hat{\mathbf{s}}_i \cdot \left(J\sum_{j\in i} \tilde{\mathbf{m}}_j + \mu\mathbf{B}\right), \tag{3}$$

where the expression in the parentheses

$$\mu\mathbf{B}_i^{\text{e}} = J\sum_{j\in i} \tilde{\mathbf{m}}_j + \mu\mathbf{B} \tag{4}$$

is the effective field acting on the mean-field spin moment $\tilde{\mathbf{m}}_i$ due to its neighbors j and is derived as the variational derivative with respect to $\tilde{\mathbf{m}}_i$. The notation $j \in i$ means the summation is carried out over all interacting neighbors j of the spin i. The mean-field spin moment $\tilde{\mathbf{m}}_i$ can be evaluated from Eq. (3) using the canonical statistical mechanics:

$$\tilde{\mathbf{m}}_i = \frac{\text{Tr}_{\mathbf{s}_i}\mathbf{s}_i \exp\left(-\beta\mathcal{H}_{\text{MF}}\right)}{\text{Tr}_{\mathbf{s}_i}\exp\left(-\beta\mathcal{H}_{\text{MF}}\right)}. \tag{5}$$

Note that since $\tilde{\mathbf{m}}$ is no longer a unit vector, Eq. (3) no longer conforms with the usual Heisenberg definition of the

TABLE I. VAMPIRE MC parameters.

Grain size (nm)	Equilibration step	Total time step
1.0–1.5	5×10^7	2.5×10^8
2.0–2.5	10^7	10^8
3.0–5.5	10^6	10^7
$\geqslant 6.0$	10^5	10^6

exchange. However, if we transform to unit vectors by multiplying through by $|\tilde{\mathbf{m}}|^2/|\tilde{\mathbf{m}}|^2$ we are left with the prefactor of the summation term in Eq. (3) as $J\tilde{\mathbf{m}}^2$ which represents the temperature dependence of the effective exchange in the mean-field sense [23]. Considering that stable moment configurations are aligned with their effective fields, i.e., $\tilde{\mathbf{m}}_i \parallel \tilde{\mathbf{B}}_i^{\mathrm{e}}$, allows expressing $\tilde{\mathbf{m}}_i$ as

$$\tilde{\mathbf{m}}_i = \mathcal{L}\big(\beta\mu|\tilde{\mathbf{B}}_i^{\mathrm{e}}|\big)\frac{\tilde{\mathbf{B}}_i^{\mathrm{e}}}{|\tilde{\mathbf{B}}_i^{\mathrm{e}}|}. \tag{6}$$

Here $\mathcal{L}(x) = \coth x - x^{-1}$ is the Langevin function, and $\beta = (k_B T)^{-1}$ with k_B being the Boltzmann constant and T the temperature. Equations (4) and (6) represent a set of coupled nonlinear algebraic equations which can be solved iteratively in a straightforward way, as discussed elsewhere [22].

III. RESULTS AND DISCUSSION

We have investigated the temperature-dependent magnetic properties of a material with the Curie temperature of FePt as a function of the grain size. Our simulations are carried out using the VAMPIRE atomistic simulation software package [24,25]. In VAMPIRE simulations, a METROPOLIS Monte Carlo (MC) integrator is used to compute the value of normalized mean magnetization length $M(T)$ as a function of temperature. The Curie temperature T_C is computed from locating the extrapolated peak of the mean longitudinal susceptibility $\chi(T)$ as function of temperature [26]. Simulations are repeated 20 times to compute statistical average and standard deviation of the Curie temperature. For each repeat, a randomly generated set of initial conditions is assigned so as to imitate the slightly varying initial conditions in a typical experiment. The grain size dependent MC parameters used in VAMPIRE simulations are given in Table I. A factor of potential importance has been predicted for grain sizes below 3 nm. Gruner *et al.* [27] have shown using *ab initio* calculations that the simple morphologies used here may give way to multiply twinned structures including cases where the magnetization in the core is lowered by shellwise ferrimagnetic spin arrangements. However, the freestanding grains considered in Ref. [27] differ from the grains used in HAMR media which are grown on MgO to promote c-axis ordering perpendicular to the plane. While morphological changes for small grain size cannot be ruled out, further work is required to establish their nature in sputtered media.

In this paper, we construct parallelepiped FePt grains with a nominal constant height (z) of 10 nm and square base of variable size (x, y) in a nominal range from 1 to 10 nm in 0.5-nm increments. The unit cells of all configurations of FePt, following Mryasov *et al.* [13], have dimensions of $x_0 =$

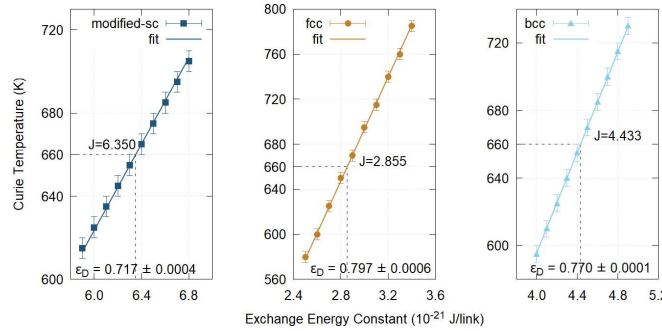

FIG. 2. Determination of the exchange energy constant for grains with different lattice structures. As expected there is a linear dependence of the Curie temperature on the exchange strength. By interpolation we determine the exchange energy to give a consistent $T_C = 660$ K for each lattice structure. The analytical finite-size correction factor ϵ_D which is calculated from the extracted gradient is shown at the bottom for each case.

$y_0 = 2.72$ Å and $z_0 = 3.85$ Å. To avoid creating incomplete unit cells on the grain surface, the grains are composed of integer numbers of unit cells in each dimension, so the exact xyz sizes of each grain are multipliers of x_0 closest to their corresponding nominal values. As previously mentioned, three lattice structure configurations are simulated: A modified-sc configuration representing the original fct $L1_0$-FePt, and two "artificial" fcc and body-centered-cubic (bcc) FePt configurations which for the purpose of comparison are made to share the same magnetic attributes of the original fct $L1_0$-FePt. The effects of crystal lattices are investigated with the Curie temperature in each case first preset to a theoretically calculated critical temperature of 660 K [26] in the largest grain of 10-nm base size. Although the referenced value of T_C at 660 K is slightly lower than commonly reported experimental values, it does not affect qualitative behaviors and analysis of results because in our investigation the Curie temperature T_C is linearly dependent on the exchange energy strength J_{ij} [28] given by

$$J_{ij} = \frac{3k_B T_C}{\epsilon z}, \tag{7}$$

where k_B is the Boltzmann constant, z is the number of nearest-neighbor interactions in a unit cell, and ϵ is the correction factor relating to the coordination-dependent spin wave stiffness. Both z and ϵ are uniquely determined for each lattice structure, and the values of ϵ for an infinite system – denoted ϵ^{∞} – can be found in previous literature [25,28]. Since the exchange interaction in our simulations is set to involve only nearest neighbors, the exchange interaction strength J_{ij} between each pair of nearest neighbors can reasonably be assumed to be similar. Therefore, J_{ij} can henceforth be simplified to the exchange energy constant J. Note that Eq. (7) can also be derived from the mean-field theory, as shown in the Supplemental Material Sec. S1 [29]. Generally, the fact that for a given structure the critical temperature T_C varies linearly with the next-neighbor interaction J simply reflects the elementary property that, for a fixed Hamiltonian and lattice structure, the statistical-mechanical treatment always involves T and J only in the combination $(k_B T)/J$. This property remains true for both mean-field calculation and numerical simulation.

TABLE II. Unit cell parameters for each simulated lattice structure of FePt.

Configuration	z	ϵ^{∞} [25,28]	J (J/link)	ϵ_D
modified-sc	6	0.719	$(6.303 \pm 0.004) \times 10^{-21}$	0.717 ± 0.0004
fcc	12	0.790	$(2.866 \pm 0.002) \times 10^{-21}$	0.797 ± 0.0006
bcc	8	0.766	$(4.430 \pm 0.002) \times 10^{-21}$	0.770 ± 0.0001

For a specific lattice structure, J is determined computationally by interpolation to give a consistent $T_C = 660$, K for each lattice structure as shown in Fig. 2. The linear variation of T_C on J obtained in Fig. 2 validates Eq. (7). Following Eq. (7), the gradient of each line is given by $(\epsilon_D z)/3k_B$ where ϵ_D is the numerical value of ϵ for a finite-size system. Table II provides literature values of z and ϵ^{∞}, as well as numerical J and ϵ_D. As can be seen, the calculated values of finite-size ϵ_D agree very well with infinite-size ϵ^{∞}, which implies that the interpolated value of exchange energy J obtained for each lattice structure is sufficiently precise. Other parameters representing magnetic properties of FePt which are shared by all three simulated crystal lattice configurations include the atomic spin moment μ_S and uniaxial anisotropy constant k_u, which are fixed at $3.23\mu_B$ and 2.63×10^{-22} J/atom, respectively [30]. The Curie temperature variation with grain size $T_C(D)$ is described by the finite-size scaling law (FSSL) [17,31]:

$$T_C(D) = T_C(\text{bulk})(1 - x_0 D^{-1/\nu}), \tag{8}$$

where D is the characteristic grain size, ν is a critical exponent, and x_0 is a fitting parameter on the order of the lattice spacing. Equation (8) is applied to determine x_0 and ν as well as the bulk Curie temperature T_C(bulk). The percentage Curie temperature decrease, $\Delta T_C(D)$, can then be defined as the percentage difference between the Curie temperature at each grain size $T_C(D)$ and the bulk Curie temperature T_C(bulk) obtained from the FSSL fit:

$$\Delta T_C(D) = \frac{T_C(\text{bulk}) - T_C(D)}{T_C(\text{bulk})} = x_0 D^{-1/\nu}. \tag{9}$$

It is important to note that fits to the FSSL often give values of ν which differ, in apparent contradiction to the nature of ν as a universal exponent. As a result, ν^{-1} is often replaced by a so-called shift exponent λ which may or may not agree with ν depending on the various system properties. Here we will propose a possible mechanism for the deviation from the critical exponent.

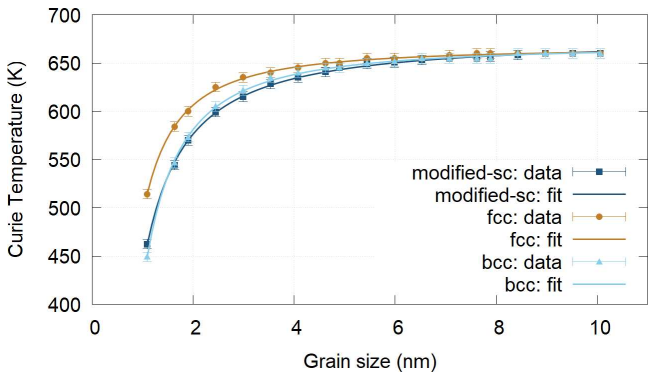

FIG. 3. The dependence of Curie temperature on grain size fits well with the FSSL for all three simulated lattice structures. The T_C increases sharply at smallest grain sizes and converges to the bulk value from around 4 nm.

We proceed to an investigation of the finite-size dependence of the Curie temperature using the atomistic model outlined earlier. Figure 3 demonstrates that the dependence of the Curie temperature on size $T_C(D)$ fits well to the FSSL [31] given in Eq. (8), consistent with previous experimental data [18]. Numerical values extracted from the FSSL for the critical exponents x_0 and ν as well as the bulk Curie temperature T_C(bulk) are given in Table III. We note that, although the FSSL fits the data well for all grain sizes investigated, the values found for ν do not agree with the expected value of 0.7 for the Heisenberg model [18,32]. Let us consider how the FSSL is obtained. It follows from the correlation scaling relation $\xi \sim (1 - T/T_C)^{-\nu}$ [33] which leads to the scaling law, Eq. (9). Note that this scaling relation for ξ is valid only for bulk systems, leading, in fitting to experimental data, to the empirical replacement of the exponent ν, which is universal, by the shift exponent λ which is nonuniversal and may include corrections to scaling. Here we consider the possibility that, for small grain sizes, the correlation length becomes dependent on the characteristic size as a result of the rescaling of system energies resulting from the fluctuations.

To provide further insight we have carried out a detailed analysis of the layer-resolved magnetization profiles which are obtained by averaging the spins in each layer. Examples of the magnetization profile at 550 K in the x direction along the grain depth are given in Fig. 4 for different grain sizes. It has to be remarked that in principle any temperature below T_C can be chosen to yield similar qualitative behaviors. In Fig. 4, M/M_s is the magnetization normalized to M_s the grain saturated magnetization at 0 K. The Atomistic Layer Index refers to lattice layers in the x direction of the grain base along the entire grain height. In larger grains (9.0 nm) surface disorder (low magnetization) causing the drop in magnetization is seen to penetrate only a few layers inside the grain. In contrast, in smaller grains where the total number of layers is reduced to the 10–12 range, surface effects begin to dominate. Our calculation shows that in smaller-sized grains the loss of order causing the decrease of Curie temperature across surface

TABLE III. FSSL fitting parameters for each simulated configuration of FePt.

Configuration	T_C(bulk) (K)	x_0	ν
modified-sc	674.2 ± 1.1	0.352 ± 0.002	0.783 ± 0.014
fcc	666.2 ± 0.7	0.260 ± 0.002	0.651 ± 0.013
bcc	668.3 ± 0.9	0.375 ± 0.003	0.656 ± 0.011

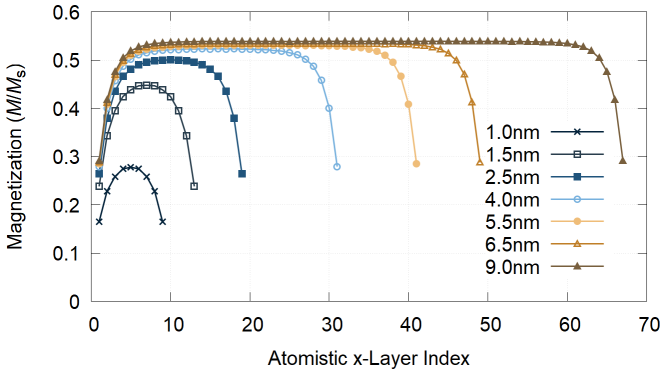

FIG. 4. The layer-resolved magnetization profile for fcc lattice grains of selected sizes at 550 K shows that in smaller grains (fewer atomistic layers) the magnetization drop on the surface contributes more to the overall loss of the grain magnetization. Note that the Atomistic x-Layer Index refers to lattice layers in the x direction of the grain base.

layers propagates into the center of the grain, an effect potentially responsible for causing a larger overall drop in the Curie temperature of the whole grain. Here we present results for the fcc lattice; results for modified-sc and bcc lattices are shown in Supplemental Material Sec. S2 [29], where in Fig. 1(b) it is shown that there is a periodic behavior for the bcc lattice, which is a physical effect arising from atoms having different numbers of nearest neighbors. Interestingly this persists to elevated temperatures in the bulk of the grain albeit somewhat reduced at the grain boundaries, supporting the idea that the disorder propagates inward from the surfaces.

The results obtained from atomistic simulations are next compared with calculations from the mean-field model described in the theory. Note that here the magnetization M/M_s is normalized to $M_s(550\ \mathrm{K})$ the magnetization of the central bulk layer at 550 K. This is done for the purpose of comparison since mean-field calculation usually yields different values of magnetization from those obtained from the atomistic model, but the overall qualitative behaviors remain similar. Two regimes of behavior for small and large grain size can be seen in Fig. 5. Particularly, the larger grains retain order in the central region, with increasing loss of order close to the surface, whereas for the smaller grains the disorder essentially penetrates the whole grain. The mean-field model gives good qualitative agreement with the atomistic model calculations, supporting the localization of the disorder close to the surface of the grain. In the following we present a simple analysis designed to characterize the penetration depth of the disordered region.

The evolution of the cross-sectional magnetization profile for fcc lattice grains at 550 K in Fig. 6 shows a decrease of magnetization across the grain surface which appears to be more pronounced in smaller grains, consistent with the data shown in Fig. 4. Here the magnetization of each point is averaged in the z direction. Results for modified-sc and bcc lattices are given in the Supplemental Material Sec. S3 [29]. These patterns suggest that surface disorder might be an important contribution to the rapid drop in T_C at smaller sizes as captured before by the FSSL: The hypothesis is that the propagation of the surface disorder into the grain has an effect on the correlation length such that $\xi = \xi(D)$. This hypothesis is consistent with the effects of a term corresponding to renormalization of state energies resulting from fluctuations [20] thereby modifying the correlation length. However, in Fig. 4 it is clear that the renormalization of the state energies decreases with distance away from the surface.

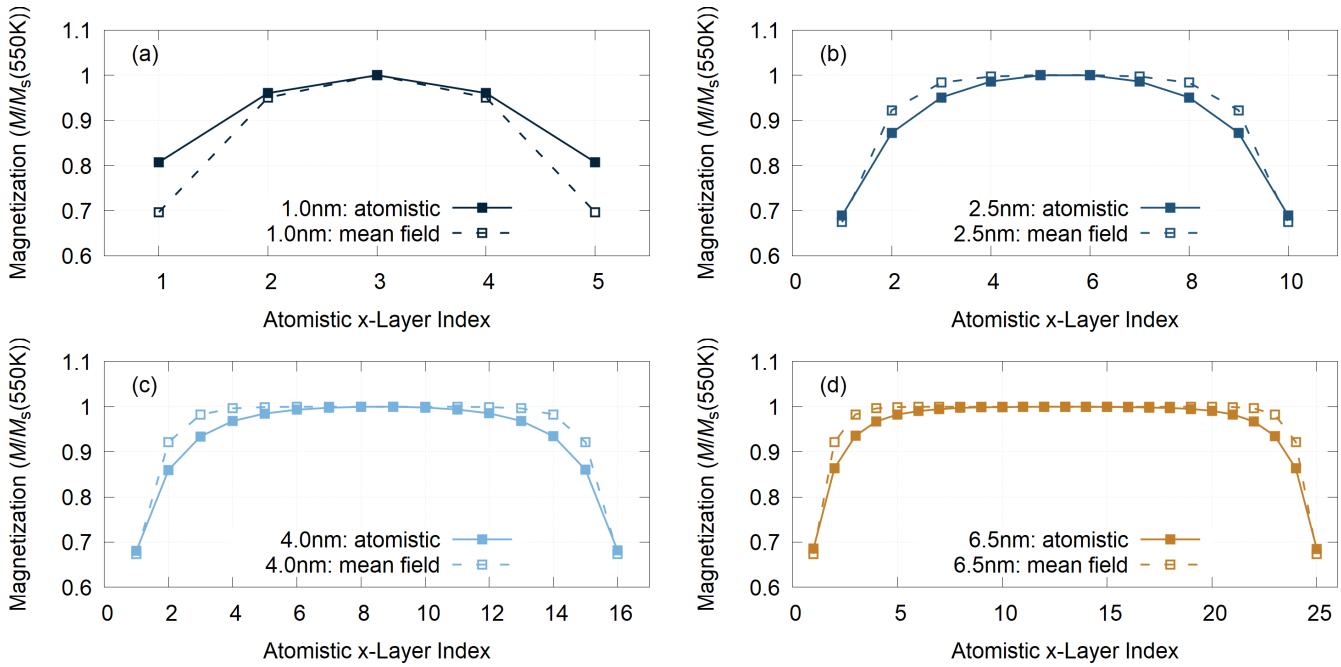

FIG. 5. Comparison between atomistic and semianalytic mean-field calculation of layer-resolved magnetization at 550 K for grains of size (a) 1.0, (b) 2.5, (c) 4.0, and (d) 6.5 nm. Note that the magnetization is normalized to $M_s(550\ \mathrm{K})$ the magnetization of the central bulk layer at 550 K. A good agreement is shown between two models, with a slight disparity occurring at the outermost surface layers of each grain.

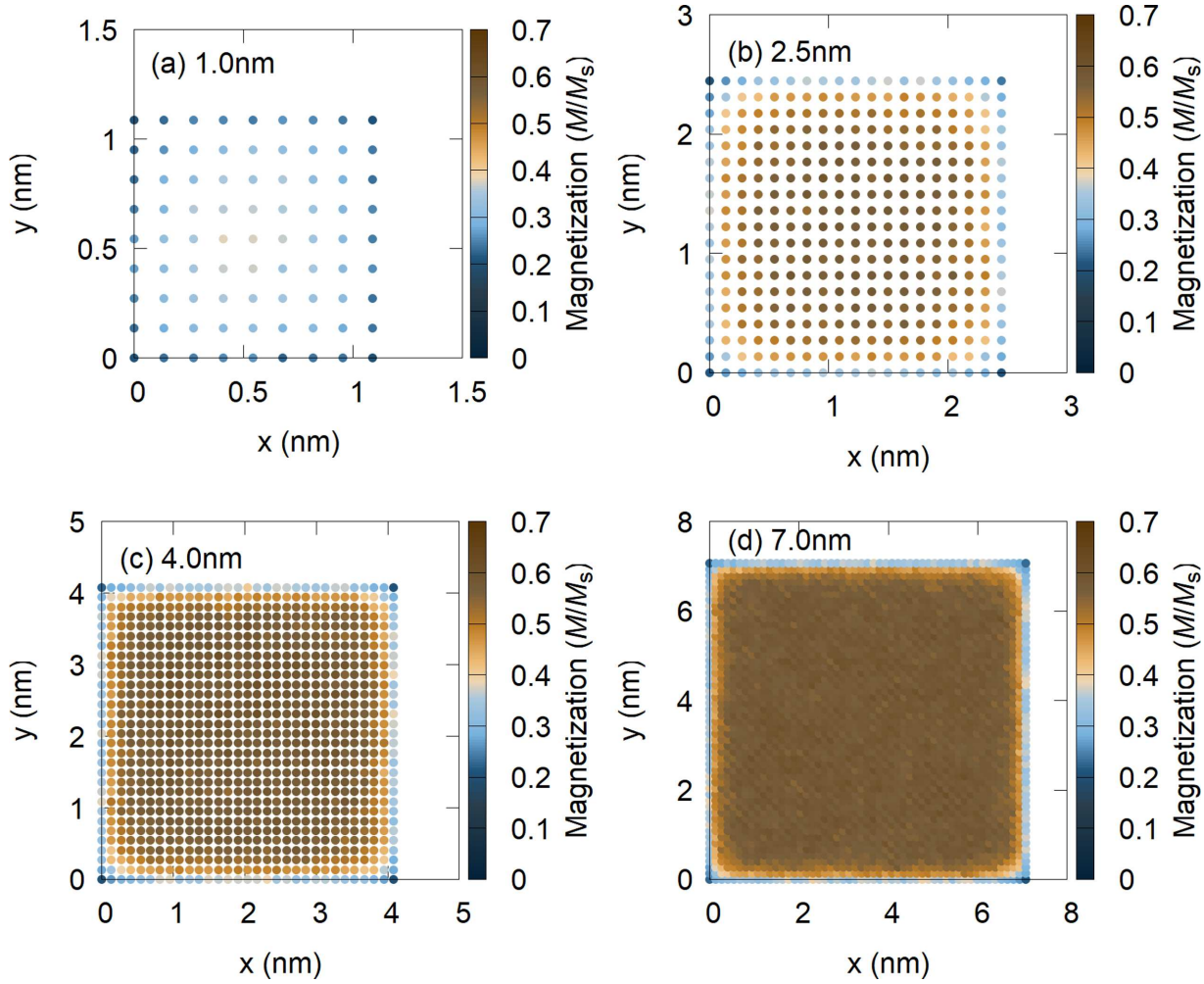

FIG. 6. Evolution of the cross-sectional magnetization profile for fcc lattice grains at 550 K of (a) 1.0, (b) 2.5, (c) 4.0, and (d) 7.0 nm in size. Note that the magnetization of each point is averaged in the z direction. The grain magnetization can be seen to be decreasing across the grain surface.

We now develop a simple analysis reflecting both contributions. The starting point is to assume that the Curie temperature reduction is entirely due to the loss of coordination at the surface. Thus ΔT_C is assumed proportional to the number of surface bonds broken. As a first approximation we assume that the number of broken bonds n_{BB} is proportional to the surface area of the grains. Then it is straightforward to show that the fractional increase in broken bonds Δn_{BB} (relative to the number of bonds in the bulk) as a function of diameter is given by

$$\Delta n_{\mathrm{BB}} = B(h^{-1} + 2D^{-1}), \tag{10}$$

where h is the height of the grain and B is a constant depending on the crystal structure and is determined by fitting to the numerical calculation. Equation (10) gives a good fit to the numerical results for all lattice structures studied, as shown in the inset of Fig. 7(a). In terms of fitting to the values of ΔT_C, we find that the assumption of $\Delta T_C \propto \Delta n_{\mathrm{BB}}$ with Δn_{BB} following the expression in Eq. (10) is valid only for large diameters, indicating that in this regime the decrease in T_C is essentially a surface effect. As we show later, for small diameter the surface disorder propagates into the center of the grain leading to a more rapid decrease of T_C, albeit one which is captured by the finite-size scaling law. We quantify this by fitting to a modified function:

$$\Delta T_C = \alpha \exp(-D/D_p) + \beta \Delta n_{\mathrm{BB}}, \tag{11}$$

where α and β are fitting constants and D_p is a characteristic distance for exponential decay associated with the propagation of the disorder into the center of the grain. As shown in Fig. 7(a), Eq. (11) fits well to the numerical calculation for all lattice structures. Values of the fitting constants are given in Table IV.

TABLE IV. Correlation fitting parameters for each simulated lattice structure of FePt.

Configuration	α	D_p (nm)	β
modified-sc	54.4 ± 2.7	1.049 ± 0.046	0.779 ± 0.034
fcc	59.4 ± 4.3	0.846 ± 0.046	0.386 ± 0.031
bcc	83.1 ± 4.4	0.863 ± 0.035	0.368 ± 0.022

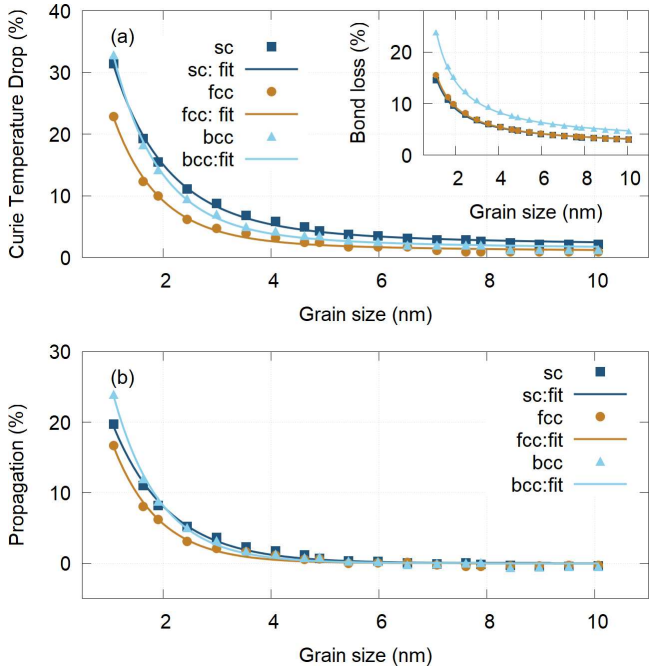

FIG. 7. Correlation between the Curie temperature drop and atomistic bond loss for each lattice structure. (a) $\Delta T_C(D)$ following from the FSSL fit and the inset showing the percentage bond loss. (b) The surface-effects propagation term ΔT_{cp} showing a cutoff value at $D \approx 3.5$ nm for all three studied lattice structures.

We define a propagation term representing the propagation of surface disorder into the grain as follows:

$$\Delta T_{Cp} = \Delta T_C - \beta \Delta n_{\mathrm{BB}}. \tag{12}$$

Equation (12), along with the numerical calculation, is shown in Fig. 7(b). It can be seen that, for diameter $D \lessapprox 3.5$ nm, there is an exponential increase in ΔT_C as the diameter decreases. Note that the cutoff value of 3.5 nm can be interpreted as the penetration depth of surface magnetization loss into the grain bulk. It is approximately four times D_p, which from Eq. (11) corresponds to approximately 1.8% of Curie temperature drop. Clearly the surface bonds lost drive the loss of magnetic order and the reduction in T_C. However, it is important to note the role played by the renormalization of the state energies arising from the fluctuations originating at the surface. This gives rise to the progressive decrease of the loss of magnetization when moving toward the center of the grain. For small grain sizes $D \leqslant 3.5$ nm, the decrease in magnetic order due to state energy renormalization cannot be stabilized by a fully ordered central core. In this regime the state energy renormalization becomes the dominant factor leading to a rapid collapse of the magnetization and T_C. Hovorka *et al.* [18] have given an expression relating the dispersion of T_C directly to the dispersion of diameter. This suggests that for decreasing grain sizes, such as expected for the evolution of HAMR, any grain size variation would give an increasingly large distribution of T_C which could become a limiting factor for the technology. On the other hand, numerous designs for HAMR media involve coupling layers with high anisotropy and low T_C with layers of lower anisotropy and higher T_C. It is likely, from the analysis presented here, that for strongly exchange coupled layers the surface disorder and hence reduction of the T_C of the high anisotropy could be somewhat mediated by the proximity effect of a higher T_C layer.

IV. CONCLUSION

We have investigated finite-size effects in small grains. Simulation data fit to the classic finite-size scaling law and show a rapid decrease of T_C at small sizes. We show that this is due to the propagation of surface disorder resulting from the loss of exchange coordination at the surface into the grain. This effect becomes important at grain sizes smaller than 4 nm and is supported by semianalytic mean-field calculation. Our findings overall are consistent with the mean-field calculation and have been extended to incorporate different crystal structures, which strongly suggests that if using a suitable correlation factor the T_C distribution of a generic material can be correlated to the percentage of atomistic bond loss on the surface as a universal parameter. The reduction of T_C is driven by surface magnetic disorder resulting from the loss of exchange coordination at the surface. These fluctuations cause a renormalization of state energies through which the magnetic disorder propagates into the grain. A physically reasonable expression is proposed which separates the two processes, and defines a penetration depth for the propagation of disorder into the grain. For small grain sizes less than around 3–4 nm, the decrease in magnetic order due to state energy renormalization cannot be stabilized by a fully ordered central core. In this regime the state energy renormalization becomes the dominant factor leading to a rapid collapse of the magnetization and T_C and a consequent increase of the dispersion of T_C for small diameter. From the viewpoint of materials design for nanoscale applications such as spintronics and particularly heat-assisted magnetic recording, finite-size effects will become an increasingly important consideration with decreasing device size. Because of the strong surface effects on the decrease of T_C, the increased T_C dispersion for small grains could be somewhat mediated in designs coupling low T_C hard materials such as FePt with high T_C materials which would reduce the loss of magnetic order through the proximity effect.

ACKNOWLEDGMENTS

Financial support of the Advanced Storage Research Consortium (ASRC) is gratefully acknowledged. Numerous simulations for this work were undertaken on the Viking Cluster, which is a high performance compute facility provided by the University of York. We are grateful for computational support from the University of York High Performance Computing service, Viking and the Research Computing team.

[1] H. J. Richter, The transition from longitudinal to perpendicular recording, J. Phys. D **40**, R149 (2007).

[2] R. F. L. Evans, R. W. Chantrell, U. Nowak, A. Lyberatos, and H.-J. Richter, Thermally induced error: Density limit

for magnetic data storage, Appl. Phys. Lett. **100**, 102402 (2012).

[3] R. Rottmayer, S. Batra, D. Buechel, W. Challener, J. Hohlfeld, Y. Kubota, L. Li, B. Lu, C. Mihalcea, K. Mountfield, K. Pelhos, C. Peng, T. Rausch, M. Seigler, D. Weller, and X.-M. Yang, Heat-assisted magnetic recording, IEEE Trans. Magn. **42**, 2417 (2006).

[4] T. W. McDaniel, Ultimate limits to thermally assisted magnetic recording, J. Phys.: Condens. Matter **17**, R315 (2005).

[5] M. H. Kryder, E. C. Gage, T. W. McDaniel, W. A. Challener, R. E. Rottmayer, G. Ju, Y. Hsia, and M. F. Erden, Heat assisted magnetic recording, Proc. IEEE **96**, 1810 (2008).

[6] D. Weller, G. Parker, O. Mosendz, A. Lyberatos, D. Mitin, N. Schmidt, and M. Albrecht, Review article: FePt heat assisted magnetic recording media, J. Vac. Sci. Technol. B **34**, 060801 (2016).

[7] H. Loc Nguyen, L. E. M. Howard, G. W. Stinton, S. R. Giblin, B. Tanner, I. Terry, A. K. Hughes, I. M. Ross, A. Serres, and J. S. O. Evans, Synthesis of size-controlled fcc and fct FePt nanoparticles, Chem. Mater. **18**, 6414 (2006).

[8] J.-U. Thiele, S. Maat, J. Robertson, and E. Fullerton, Magnetic and structural properties of FePt-FeRh exchange spring films for thermally assisted magnetic recording media, IEEE Trans. Magn. **40**, 2537 (2004).

[9] G. Barucca, T. Speliotis, G. Giannopoulos, D. Niarchos, B. Rutkowski, A. Czyrska-Filemonowicz, E. Agostinelli, S. Laureti, A. Testa, and G. Varvaro, Magnetic anisotropy phase-graded A1/$L1_0$-FePt films on amorphous glass substrates, Mater. Des. **123**, 147 (2017).

[10] T. J. Zhou, K. Cher, J. F. Hu, Z. M. Yuan, and B. Liu, The concept and fabrication of exchange switchable trilayer of FePt/FeRh/FeCo with reduced switching field, J. Appl. Phys. **111**, 07C116 (2012).

[11] F. Wang, H. Xing, and X. Xu, Overcoming the trilemma issues of ultrahigh density perpendicular magnetic recording media by $L1_0$-Fe(Co)Pt materials, SPIN **05**, 1530002 (2015).

[12] M. Nakaya, M. Kanehara, M. Yamauchi, H. Kitagawa, and T. Teranishi, Hydrogen-induced crystal structural transformation of FePt nanoparticles at low temperature, J. Phys. Chem. C **111**, 7231 (2007).

[13] O. N. Mryasov, U. Nowak, K. Y. Guslienko, and R. W. Chantrell, Temperature-dependent magnetic properties of FePt: Effective spin hamiltonian model, Europhys. Lett. **69**, 805 (2005).

[14] H. Li and J. Zhu, The role of media property distribution in HAMR SNR, IEEE Trans. Magn. **49**, 3568 (2013).

[15] J.-G. J. Zhu and H. Li, Signal-to-noise ratio impact of grain-to-grain heating variation in heat assisted magnetic recording, J. Appl. Phys. **115**, 17B747 (2014).

[16] J. Waters, D. Kramer, T. J. Sluckin, and O. Hovorka, Resolving Anomalies in the Critical Exponents of FePt using Finite-Size Scaling in Magnetic Fields, Phys. Rev. Appl. **11**, 024028 (2019).

[17] A. Lyberatos, D. Weller, and G. J. Parker, Finite size effects in $L1_0$-FePt nanoparticles, J. Appl. Phys. **114**, 233904 (2013).

[18] O. Hovorka, S. Devos, Q. Coopman, W. J. Fan, C. J. Aas, R. F. L. Evans, X. Chen, G. Ju, and R. W. Chantrell, The Curie temperature distribution of FePt granular magnetic recording media, Appl. Phys. Lett. **101**, 052406 (2012).

[19] C.-b. Rong, D. Li, V. Nandwana, N. Poudyal, Y. Ding, Z. Wang, H. Zeng, and J. Liu, Size-dependent chemical and magnetic ordering in $L1_0$-FePt nanoparticles, Adv. Mater. **18**, 2984 (2006).

[20] N. Goldenfeld, *Lectures on Phase Transitions and the Renormalization Group* (CRC, Boca Raton, FL, 2018)

[21] C. Penny, A. R. Muxworthy, and K. Fabian, Mean-field modelling of magnetic nanoparticles: The effect of particle size and shape on the curie temperature, Phys. Rev. B **99**, 174414 (2019).

[22] O. Hovorka and T. J. Sluckin, A computational mean-field model of interacting non-collinear classical spins, arXiv:2007.12777 (2020).

[23] U. Atxitia, D. Hinzke, O. Chubykalo-Fesenko, U. Nowak, H. Kachkachi, O. N. Mryasov, R. F. Evans, and R. W. Chantrell, Multiscale modeling of magnetic materials: Temperature dependence of the exchange stiffness, Phys. Rev. B **82**, 134440 (2010).

[24] https://vampire.york.ac.uk/.

[25] R. F. L. Evans, W. J. Fan, P. Chureemart, T. A. Ostler, M. O. A. Ellis, and R. W. Chantrell, Atomistic spin model simulations of magnetic nanomaterials, J. Phys.: Condens. Matter **26**, 103202 (2014).

[26] N. Kazantseva, D. Hinzke, U. Nowak, R. W. Chantrell, U. Atxitia, and O. Chubykalo-Fesenko, Towards multiscale modeling of magnetic materials: Simulations of FePt, Phys. Rev. B **77**, 184428 (2008).

[27] M. E. Gruner, G. Rollmann, P. Entel, and M. Farle, Multiply Twinned Morphologies of FePt and CoPt Nanoparticles, Phys. Rev. Lett. **100**, 087203 (2008).

[28] D. A. Garanin, Self-consistent Gaussian approximation for classical spin systems: Thermodynamics, Phys. Rev. B **53**, 11593 (1996).

[29] See Supplemental Material at http://link.aps.org/supplemental/10.1103/PhysRevB.106.054421 for the mean-field derivation of the Curie temperature, and the layer-resolved and cross-sectional magnetization profiles for the sc and bcc lattices.

[30] M. Strungaru, S. Ruta, R. F. L. Evans, and R. W. Chantrell, Model of Magnetic Damping and Anisotropy at Elevated Temperatures: Application to Granular FePt Films, Phys. Rev. Appl. **14**, 014077 (2020).

[31] J. Waters, A. Berger, D. Kramer, H. Fangohr, and O. Hovorka, Identification of Curie temperature distributions in magnetic particulate systems, J. Phys. D **50**, 35LT01 (2017).

[32] J. M. Yeomans, *Statistical Mechanics of Phase Transitions* (Oxford University, New York, 1992).

[33] A. Aharoni, *An Introduction to the Theory of Ferromagnetism* (Clarendon, Oxford, 2000).